

CoPark: Learning Reactive Parking via Self-Play

Jiarong Wei^{1,2}, Yanxing Chen³, Sinuo Song³, Yin Wu², Anna Rehr², Abhinav Valada¹

¹Department of Computer Science, University of Freiburg, Germany

²CARIAD SE, Germany

³Technical University of Munich, Germany

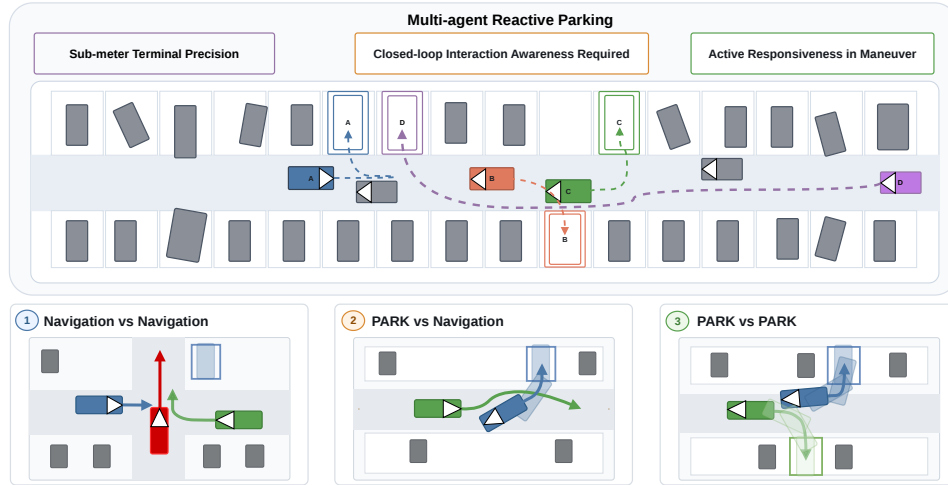


Figure 1: Reactive parking requires multiple vehicles in a shared lot to reach assigned slots from random initial poses, with strict terminal tolerance on slot pose, while remaining responsive to neighbors throughout the process. Bottom: interaction during navigation (1), parking maneuver (3), or both (2).

Abstract: Learning a single policy that reaches a goal with high geometric precision while interacting safely with nearby agents poses conflicting objectives. Precision favors commitment to a fixed geometric plan, whereas interaction requires immediate deviation when another agent intrudes, causing policies optimized for one objective to often fail at the other. We study this problem in the context of reactive autonomous parking, where multiple vehicles must reach assigned slots with sub-meter terminal accuracy while remaining responsive to neighboring vehicles throughout the maneuver. We propose CoPark, a self-play RL approach that learns reactive parking through multi-agent self-play, built on a residual-policy architecture. A precomputed offline plan provides a fixed action prior, while a residual head learns the reactive corrections. This decomposition separates geometric consistency from interaction. The residual policy learns behaviors under self-play, where data and scripting fall short, while the fixed prior holds the slot-frame geometry that pure policies struggle to reach reliably. The key design is a partner-threat-modulated, channel-asymmetric release of the prior. A continuous threat signal shifts authority of the longitudinal channel to the residual head to enable yielding, while the lateral channel remains anchored to the precomputed reference to preserve sub-meter slot alignment. A closed-loop refinement layer corrects residual terminal error from action-grid discretization. We train our policy on six parking lots and evaluate zero-shot on our new reactive-parking benchmark spanning Dragon Lake Parking (DLP) and DeepScenario Open 3D (DSC3D). CoPark achieves ~ 70 – 85% success with only 3–6% collision rate, substantially outperforming classical, imitation-learning, and large-scale RL baselines. Importantly, the results demonstrate emergent interaction behaviors such as reverse-yielding, mid-maneuver yielding, tight-corridor passing, and queuing.

Keywords: Self-play, Multi-agent planning, Reactive parking

1 Introduction

Self-play Reinforcement Learning (RL) has driven breakthroughs from board games and competitive control [1, 2, 3, 4] to autonomous driving, where large-scale multi-agent simulation and closed-loop training yield the emergence of robust behavior on held-out scenarios [5, 6, 7, 8]. These successes are concentrated in settings shaped by strong lane priors and forward-only kinematics, where sub-meter terminal accuracy is not required. Tasks that simultaneously combine high-precision maneuvers, tight spatial constraints, and low-speed multi-agent interaction remain largely unaddressed by self-play.

Reactive parking is a representative instance (Fig. 1): each vehicle must navigate from a random feasible pose to its assigned slot with parking-grade accuracy while remaining responsive to neighbors throughout the maneuver. The task jointly demands sub-meter terminal precision under non-holonomic geometry, closed-loop interaction awareness in confined aisles, and active responsiveness during the parking maneuver rather than only during routing, a combination that existing paradigms address only in part.

Meeting these requirements together is hard since they pull against one another within a single policy. Robust interaction is difficult to learn from supervision: the scarce parking-interaction data resists imitation, and the combinatorial space of multi-agent encounters resists hand-scripting, which points to self-play as the paradigm for learning interactive behavior. Precision is the opposing difficulty. A policy learned purely from reward struggles to reach parking-grade accuracy, needing elaborate curricula even in the single-agent case [9, 10], let alone while simultaneously learning to interact. Precision therefore calls for external geometric grounding beyond what reward alone discovers. This grounding, however, conflicts with reactivity: a fixed reference anchors the slot frame but, held rigidly, blocks the deviations that yielding requires. Reconciling precision and reactivity within one policy, without a behavior-specific controller for each interaction pattern, is the central challenge.

We resolve this challenge with CoPark, a self-play RL approach that learns reactive parking through multi-agent self-play. To supply precision without bottlenecking self-play, an inexpensive offline plan, a Stanley tracker over a Hybrid A* path computed once per instance, enters the action logits as a fixed prior, sidestepping the unstable, curriculum-heavy precision learning that pure policies require. To keep this prior from obstructing interaction, a residual head modulates its authority by perceived partner threat and releases it anisotropically, relaxing the longitudinal channel so the policy can yield while anchoring the lateral channel to hold slot alignment. This instantiates a general principle: a prior should be released to match a task’s anisotropic tolerance, anchored where tolerance is tight and relaxed where it is loose. A closed-loop refinement layer then continues acting after the plan ends, absorbing terminal error from action-grid discretization and partner-induced drift.

We train our policy on six parking lots and evaluate zero-shot on our new reactive-parking benchmark integrating DLP and DSC3D into PufferDrive [11]. The results demonstrate that CoPark achieves a 70–85% success rate with a 3–6% collision rate across both partner modes, substantially outperforming classical, imitation-learning, and pure large-scale RL baselines, while exhibiting emergent interaction behaviors such as reverse-yielding, mid-maneuver yielding, tight-corridor passing, and queuing.

To summarize, the main contributions are as follows:

1. We formulate reactive parking, a closed-loop multi-agent task that jointly requires parking-grade terminal precision, full-process interaction awareness, and active responsiveness during the maneuver itself, a combination no prior approach addresses jointly.
2. We propose CoPark, whose central mechanism is a partner-threat-modulated, channel-asymmetric release of an offline kinematic prior, combined with a closed-loop refinement layer for terminal precision.
3. We introduce a reactive parking benchmark that incorporates DLP and DSC3D agents into the PufferDrive simulator, with both reactive and non-reactive partner modes.
4. We present extensive evaluations showing strong zero-shot performance across both datasets, substantially outperforming representative baselines in success rate, with emergent multi-agent behaviors.

2 Related Work

Self-Play for Closed-Loop Autonomous Driving: Self-play [1, 2] has driven breakthroughs in zero-sum games [3, 4], and recent work transfers the idea to closed-loop autonomous driving. GigaFlow [5] demonstrates that robust naturalistic driving behaviors emerge when self-play is scaled to long horizons with thousands of agents and per-agent reward conditioning. CaRL [12], not itself self-play, scales a PPO planner with deliberately simple rewards to match or surpass more elaborate recipes on standard nuPlan and CARLA benchmarks. GPUDrive [6] provides a million-FPS multi-agent simulator that makes such scale practical, and Cornelisse *et al.* [7] report near-closure of the train–test gap on held-out scenarios by scaling self-play to thousands of driving scenes. Follow-up work adds KL regularization toward a human reference policy [8, 13] to keep emergent driving styles human-compatible, or introduces asymmetric teacher–student dynamics [14] that broaden the training distribution toward rare but safety-critical situations. These methods operate on open road networks where lane structure constrains the solution space and centimeter-level terminal accuracy is never demanded. Reactive parking sits in the opposite regime, demanding sub-meter terminal precision, dense low-speed interaction in confined corridors, and online responsiveness throughout the parking maneuver, none of which these large-scale recipes are built to deliver.

Prior-Guided and Residual Reinforcement Learning: A complementary line of work injects external structure into RL to meet precision requirements that pure exploration struggles to satisfy. One branch uses demonstrations or reference policies as a soft signal [15, 16, 17, 18, 19], encoding the teacher through auxiliary imitation losses or KL regularisation toward a behavioral-cloning baseline. A second branch is residual policy learning [20, 21, 22], in which a learned policy refines a fixed sub-optimal controller rather than replacing it. The residual is typically applied in action space or as a log-prior on the policy distribution under a single global reliance scalar. In parking, HOPE [23] couples an RL agent with Reeds–Shepp curves via action masking, and DRIP [24] uses an RL-pretrained prior refined by a diffusion model. Most of these methods are trained in single-ego settings with static or scripted neighbors and treat the prior as a fixed structural component whose authority does not vary with the multi-agent state. Reactive parking instead requires the prior’s authority to be modulated by partner threat and split across action channels, a form of structured prior release that prior-guided and residual RL have left unexplored.

Multi-Agent Interaction Learning for Automated Parking: Automated valet parking systems traditionally decouple multi-vehicle coordination from low-level motion. At the strategic layer, learning is applied to slot allocation [25] and joint parking-and-charging scheduling [26]. At the motion layer, coordination is handled by infrastructure-coordinated predictive control with V2I [27] or by hierarchical path planning with multi-vehicle collision avoidance [28], both depending on explicit interaction models and centralized computation. Recent multi-agent RL approaches [29, 30] jointly train multiple parking agents but focus on conflict-free planning under simplified kinematics rather than on closed-loop terminal precision. Beyond the hybrid prior-RL methods discussed above, learning-based parking is otherwise mostly single-agent [9, 10], with a parallel line modeling multi-agent parking interaction for trajectory prediction [31, 32] rather than for closed-loop control. To our knowledge, no prior work has learned interactive parking behavior across both the navigation and parking-maneuver phases under closed-loop multi-agent self-play.

3 Problem Formulation

We formulate reactive parking as a general-sum partially observable stochastic game [33] (POSG) $\langle \mathcal{N}, \mathcal{S}, \mathcal{A}, \mathcal{O}, P, R, \gamma \rangle$, where $N = |\mathcal{N}| \geq 2$ controlled vehicles share a parking lot, each pursuing its own assigned slot while remaining responsive to neighbors.

Setting: A parking lot is $\mathcal{L} = (\mathcal{D}, \mathcal{P}, \mathcal{O}_{\text{obs}}, \mathcal{G})$ with drivable region \mathcal{D} , slot poses $\mathcal{P} = \{p_m\}_{m=1}^M$, static obstacles \mathcal{O}_{obs} , and lane graph \mathcal{G} . Each vehicle i has state $s_{i,t} = (x_{i,t}, y_{i,t}, \psi_{i,t}, v_{i,t})$ under bicycle kinematics, takes a discrete action $a_{i,t} = (a_{i,t}^{\text{acc}}, a_{i,t}^{\text{steer}})$ from an acceleration–steering grid, and receives a partial observation $o_{i,t}$ of ego state, the relative state of its K nearest neighbors ($K=8$),

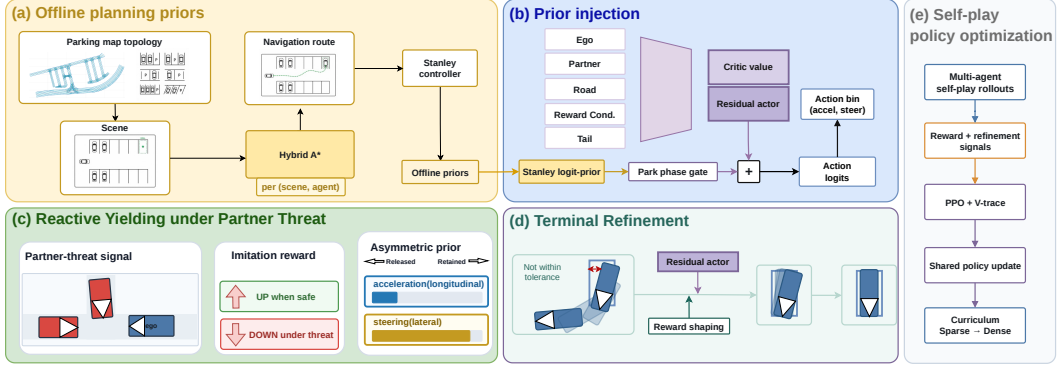


Figure 2: Architecture of CoPark. (a) Offline planning priors: Hybrid A* plan and Stanley tracker, precomputed per (scene, agent), supply a geometric reference. (b) Prior injection: a residual actor over ego, partner, road, reward-conditioning, and tail blocks adds logits to the phase-gated Stanley logit-prior. (c) Reactive yielding: the partner-threat signal modulates imitation reward and asymmetrically releases the longitudinal prior while anchoring the lateral channel. (d) Terminal refinement: the residual actor continues acting beyond plan completion under a refinement reward toward the slot frame. (e) Self-play policy optimization: multi-agent rollouts feed PPO with V-trace under a sparse-to-dense curriculum.

local geometry, and target slot pose. Vehicles start at distinct feasible initial states $s_{i,0}$ on \mathcal{D} and are assigned target slots via an injective map $\sigma : \mathcal{N} \rightarrow \{1, \dots, M\}$. Each trajectory decomposes into navigation and parking-maneuver phases.

Success and termination: In the slot-aligned frame of $p_{\sigma(i)}$, agent i succeeds when

$$\|e_{i,t}^{\text{slot}}\|_2 \leq \Delta_d, \quad |\text{wrap}_{\pi}(\psi_{i,t} - \psi_{\sigma(i)})| \leq \Delta_{\psi}, \quad |v_{i,t}| \leq \Delta_v, \quad (1)$$

holds for K_s consecutive steps. The heading is wrapped modulo π , accepting both forward-in and reverse-in orientations. Trajectories also terminate on collision (vehicle-vehicle or vehicle-static) or timeout. The per-agent reward $R(s_{i,t}, a_{i,t}, S_t)$, with joint state $S_t = \{s_{j,t}\}_{j \in \mathcal{N}}$, couples agents through terminal events and generic dense safety terms, and contains no behavior-specific rewards for yielding, queuing, or reverse-yielding.

Objective: We restrict to homogeneous parameter-sharing policies $\pi_{\theta} : \mathcal{O} \rightarrow \Delta(\mathcal{A})$ with learning objective

$$\theta^* = \arg \max_{\theta} \mathbb{E}_{(\mathcal{L}, \{s_{i,0}\}, \sigma) \sim \mathcal{Q}} \mathbb{E}_{\pi_{\theta}} \left[\sum_{i \in \mathcal{N}} \sum_{t=0}^T \gamma^t R(s_{i,t}, a_{i,t}, S_t) \right], \quad (2)$$

where \mathcal{Q} is the joint task distribution over parking lots, initial states, and slot assignments, and T is the episode horizon, with each agent’s reward set to zero after its own termination. During training, every partner in S_t is itself controlled by π_{θ} , making the optimization a multi-agent self-play process. The learned policy is ego-centric and can be deployed against arbitrary partners that need not share it (Sec. 5).

4 Method

In this section, we introduce CoPark’s four key components (Fig. 2). The offline kinematic prior (Sec. 4.1) and its residual injection (Sec. 4.2) provide terminal precision. The reactive yielding under partner threat (Sec. 4.3) keeps the policy responsive to neighbors throughout the parking maneuver, and the closed-loop refinement layer (Sec. 4.4) corrects residual terminal error. All four are trained jointly under multi-agent self-play with a scene-density curriculum (Sec. 4.5).

4.1 Offline Kinematic Prior

We precompute a fixed kinematic teacher per task instance to bootstrap the policy beyond pure self-play’s budget. For every (\mathcal{L}, i) pair, a Hybrid A* [34] search with a Reeds–Shepp [35] analytic shot

under static-only collision checks, leaving dynamic interaction to the residual, yields a navigation route on \mathcal{G} from $s_{i,0}$ to a preparation pose p_i^{prep} , sampled at uniform arc length into subgoals $\{g_{i,1}, \dots, g_{i,K_i}\}$, together with a maneuvering trajectory τ_i from p_i^{prep} to $p_{\sigma(i)}$ on the execution action grid. The subgoals shape navigation progress and τ_i supplies the reference modulated in Sec. 4.3. The agent transitions one-way from the navigation to the maneuver phase upon entering a tolerance neighborhood of p_i^{prep} , defining the phase indicator $\phi_{i,t}$ used below.

4.2 Residual Policy with Prior Injection

A single parameter-sharing categorical policy $\pi_\theta(a | s)$, where s abbreviates the ego observation $o_{i,t}$ of Sec. 3, acts at every step of both phases, with the offline prior engaged only during the parking maneuver. The teacher trajectory τ_i is read by a Stanley controller [36] which emits a target command $(\hat{a}_{i,t}, \hat{\delta}_{i,t})$, encoded as a pair of per-channel Gaussian log-priors $\log p_{\text{prior}}^{\text{acc}}$ and $\log p_{\text{prior}}^{\text{steer}}$ over the 7×13 acceleration–steering action grid and added to the policy logits:

$$\log \pi_\theta(a | s) \propto z_\theta(s, a) + \mathbf{1}[\phi_{i,t} = \text{Maneuver}] (\alpha^{\text{acc}}(s) \log p_{\text{prior}}^{\text{acc}}(a) + \alpha^{\text{steer}}(s) \log p_{\text{prior}}^{\text{steer}}(a)), \quad (3)$$

with $z_\theta(s, a)$ a bounded residual logit head and $\alpha^{\text{acc}}(s)$, $\alpha^{\text{steer}}(s)$ channel-wise reliance scalars derived from a learned base $\alpha(s) \in [\alpha_{\min}, \alpha_{\max}]$. The Stanley controller never writes to the simulator; the reference enters only as a structural pull on the policy distribution, whose dynamics under partner threat are defined in Sec. 4.3.

4.3 Reactive Yielding under Partner Threat

The prior pull of Eq. 3 must relax in proportion to partner activity, asymmetrically across the two action channels, and continuously rather than in switched modes.

Partner-threat signal: We summarize the instantaneous interaction state of agent i by

$$\text{threat}_i = \sum_{j \in \mathcal{N}_K(i)} [-\dot{d}_{ij}]_+ \exp(-d_{ij}/d_{\text{decay}}), \quad (4)$$

aggregating per-partner contributions over the K nearest neighbors $\mathcal{N}_K(i)$ that form the partner block of the observation (Sec. 3). Each contribution combines the rectified closing rate $[-\dot{d}_{ij}]_+ = \max(0, -\dot{d}_{ij})$, where $d_{ij} = \|p_i - p_j\|_2$ is the ego–partner distance and \dot{d}_{ij} its time derivative, with an exponentially decaying range envelope. The signal enters the per-step reward as a dense closing penalty $-\beta_{\text{dyn}} \text{threat}_i$, and is mapped into a saturated interaction intensity through a smooth squash,

$$\rho(s) = 1 - \exp(-\text{threat}_i/\tau_\rho) \in [0, 1],$$

rising continuously from 0 in the empty lot toward 1 under sustained dense interaction.

Threat-modulated imitation reward: The Stanley command also enters as a behavior-cloning reward, with weight relaxed continuously by $\rho(s)$:

$$r_{i,t}^{\text{imit}} = \alpha_{\text{imit}} (1 - \rho(s)) w_{\text{trust}}(s) \exp(-\|u_{i,t} - \hat{u}_{i,t}\|_2/\sigma_{\text{imit}}), \quad (5)$$

where $u_{i,t}, \hat{u}_{i,t} \in [-1, 1]^2$ are the per-channel-normalized policy and teacher commands and $w_{\text{trust}}(s) \in [0, 1]$ is the multiplicative trust-weight

$$w_{\text{trust}}(s) = \underbrace{\exp(-\|e_{\text{ct}}(s)\|/\sigma_{\text{ct}})}_{\text{cross-track suppression}} \cdot \underbrace{\sigma(\beta_{\text{stat}}(d_{\text{stat}}(s) - d_0))}_{\text{static-clearance gate}} \cdot \underbrace{\max(0, 1 - \xi(s))}_{\text{plan-progress decay}}, \quad (6)$$

combining teacher cross-track error $e_{\text{ct}}(s)$, distance to the nearest static edge $d_{\text{stat}}(s)$, and the teacher’s plan-progress fraction $\xi(s) \in [0, 1]$ (σ is the logistic sigmoid). The imitation signal therefore never penalizes legitimate safety deviations and vanishes once the teacher has finished its plan.

Asymmetric channel-wise prior modulation: The reliance scalars of Eq. 3 contract along the same $\rho(s)$ but at different rates per channel,

$$\alpha^c(s) = \alpha(s) (1 - \kappa^c \rho(s)), \quad c \in \{\text{acc}, \text{steer}\}, \quad (7)$$

with $\kappa^{\text{acc}} \gg \kappa^{\text{steer}}$ as the only design asymmetry. The longitudinal prior relaxes toward $\alpha(s)(1 - \kappa^{\text{acc}})$, handing authority to the residual to brake, hold, or reverse, while the lateral prior persists near $\alpha(s)(1 - \kappa^{\text{steer}})$, anchoring the slot frame. Appendix C.1 shows that the channel asymmetry $\kappa^{\text{acc}} - \kappa^{\text{steer}}$, not the release magnitude, is the operative design choice.

4.4 Closed-Loop Terminal Refinement

A single rollout of π_θ through τ_i rarely lands within the success tolerance of Eq. 1 due to action-grid discretization and yielding-induced drift. We let the same π_θ continue acting beyond plan completion; once arc progress along τ_i stalls and the agent remains outside tolerance, the per-step reward switches to

$$\tau_{i,t}^{\text{ref}} = \beta_{\text{red}} \eta \tanh((\|e_{i,t-1}^{\text{slot}}\|_2 - \|e_{i,t}^{\text{slot}}\|_2)/\eta) + \beta_{\text{hold}} \mathbf{1}[e_{i,t}^{\text{slot}} \in \mathcal{E}_{\text{tol}} \wedge |v_{i,t}| \leq \Delta_v], \quad (8)$$

where \mathcal{E}_{tol} is the pose tolerance set from Eq. 1 and η is the tanh saturation scale. The first term is a smoothly saturating directed gradient toward the slot, bounded by $\pm\beta_{\text{red}}\eta$. The second is a hold bonus toward the K_s -step consecutive hold of the success criterion. Refinement ends in success when Eq. 1 holds for K_s steps and in failure when the budget $K_{\text{ref}}^{\text{max}}$ is exhausted. The imitation reward of Eq. 5 is naturally suppressed inside refinement since the teacher’s plan has terminated.

4.5 Self-Play Policy Optimization

We optimize π_θ under multi-agent self-play with per-agent reward conditioning following GigaFlow’s [5] recipe. Training uses PPO [37] with V-trace [38] advantages through PufferLib [39]. A single parameter set θ is shared across phases, agents, and episodes. Scenes are sampled under a sparse-to-dense scene-density curriculum set at data-preparation time (Appendix A.1). The phase information enters only through $\phi_{i,t}$ in $o_{i,t}$ and the phase-conditional prior of Eq. 3. Completed agents are removed from the rollout on termination.

5 Reactive Parking Benchmark

For zero-shot evaluation of policies trained on custom layouts, we integrate Dragon Lake Parking (DLP) [40] and DeepScenario Open 3D (DSC3D) [41] into the PufferDrive [11] simulator under Sec. 3, extracting every source-data parking trajectory as one ego-episode. This turns real logged parking trajectories, which carry no interaction protocol of their own, into the first closed-loop, reactive evaluation setting for multi-agent parking. Following GigaFlow’s [5] closed-loop protocol, each method controls a single ego while non-ego partners run in one of two scripted modes: reactive (IDM [42] along logged routes, decelerating in response to the ego) and non-reactive (log replay regardless of the ego), a self-play partners mode is reported for CoPark in Appendix C.5. Each episode is scored on seven metrics: SR, Coll, and Off as ranking metrics over all episodes; PErr and HErr as terminal-precision metrics over each method’s successful subset, and Path and Manv as diagnostic metrics read jointly with SR and Coll. Tolerances, the 91-way action interface, and other implementation details are in Appendix B.

6 Experimental Results

In this section, we empirically validate CoPark on the reactive parking benchmark of Sec. 5, characterize its emergent multi-agent behaviors, and ablate each design choice.

6.1 Training Setup and Baselines

Training Setup: We train CoPark under multi-agent self-play on 2 NVIDIA RTX A6000 GPUs for 4×10^9 environment steps, sustaining 120k simulator steps per second at episode length 400, using six custom parking-lot layouts pre-generated into 1024 scenes with a three-tier scene-density curriculum (0.25/0.5/0.75 occupancy). More details are presented in Appendix A.1. We evaluate zero-shot on the benchmark of Sec. 5 under both partner modes.

Baselines: Seven baselines span three classical planners (RS [35], Hybrid A* [34], MA-MPC [27]), an interaction-aware parking RL method (HOPE [23]), two large-scale RL recipes (GigaFlow [5], CaRL [12]), and an imitation-learning planner (Diffusion Planner [43], marked † because it is trained directly on DLP/DSC3D demonstrations and is therefore not zero-shot). Adaptation details are presented in Appendix B.5.

Partner	Method	DLP [40]							DSC3D [41]						
		SR [%]	Path [m]	Manv	PErr [m]	HErr [°]	Coll [%]	Off [%]	SR [%]	Path [m]	Manv	PErr [m]	HErr [°]	Coll [%]	Off [%]
Reactive Agents	RS [35]	5.8	17.9	1.7	0.1	0.8	64.9	5.6	7.9	11.2	0.5	0.1	0.6	64.8	6.4
	Hybrid A* [34]	11.2	22.4	0.9	0.1	1.0	57.6	1.2	6.9	16.4	0.6	0.1	0.8	59.7	1.8
	MA-MPC [27]	58.5	35.2	1.3	0.2	1.5	10.2	0.5	46.8	24.2	1.0	0.2	1.7	13.0	0.8
	HOPE [†] [23]	24.8	41.5	8.4	0.2	2.2	38.2	1.5	8.4	26.5	5.9	0.3	3.8	52.6	2.5
	GigaFlow [5]	50.8 \pm 1.7	43.8 \pm 1.4	1.1 \pm 0.1	0.5 \pm 0.1	5.5 \pm 0.5	3.8 \pm 0.7	0.8 \pm 0.2	45.5 \pm 1.6	27.5 \pm 1.0	1.2 \pm 0.1	0.5 \pm 0.1	5.8 \pm 0.5	3.3 \pm 0.8	1.2 \pm 0.3
	CaRL [12]	45.0 \pm 1.7	42.5 \pm 1.4	1.2 \pm 0.1	0.5 \pm 0.1	6.0 \pm 0.5	4.5 \pm 0.7	1.0 \pm 0.2	40.0 \pm 1.6	26.4 \pm 1.0	1.3 \pm 0.1	0.5 \pm 0.1	6.2 \pm 0.5	4.0 \pm 0.8	1.5 \pm 0.3
	Diffusion Planner [‡] [43]	54.6 \pm 1.5	25.8 \pm 0.8	1.7 \pm 0.1	0.3 \pm 0.0	2.5 \pm 0.2	10.5 \pm 1.0	0.5 \pm 0.2	48.9 \pm 1.6	19.8 \pm 1.0	1.7 \pm 0.1	0.3 \pm 0.0	2.5 \pm 0.2	13.2 \pm 1.2	0.8 \pm 0.3
CoPark (Ours)	84.7 \pm 1.4	47.6 \pm 0.6	1.7 \pm 0.2	0.4 \pm 0.0	3.9 \pm 0.2	4.1 \pm 0.7	0.0 \pm 0.0	75.8 \pm 1.7	29.6 \pm 0.5	1.7 \pm 0.2	0.4 \pm 0.0	3.3 \pm 0.2	3.5 \pm 0.8	0.0 \pm 0.0	
Non-Reactive Agents	RS [35]	3.9	18.0	1.7	0.1	1.0	77.8	6.2	5.5	11.3	0.5	0.1	0.7	71.7	6.9
	Hybrid A* [34]	8.0	22.6	0.9	0.1	1.2	66.7	1.5	4.9	16.5	0.6	0.1	0.9	65.7	2.1
	MA-MPC [27]	49.0	34.6	1.3	0.2	1.6	16.5	0.7	38.5	23.7	1.0	0.2	1.8	19.5	1.1
	HOPE [†] [23]	19.8	41.7	8.4	0.2	2.5	45.1	1.8	6.5	26.6	6.0	0.3	4.2	58.3	3.0
	GigaFlow [5]	47.8 \pm 1.7	44.0 \pm 1.4	1.1 \pm 0.1	0.5 \pm 0.1	5.8 \pm 0.5	5.2 \pm 0.8	1.1 \pm 0.3	41.9 \pm 1.6	27.7 \pm 1.0	1.2 \pm 0.1	0.5 \pm 0.1	6.0 \pm 0.5	5.5 \pm 0.9	1.5 \pm 0.3
	CaRL [12]	42.0 \pm 1.7	42.7 \pm 1.4	1.2 \pm 0.1	0.5 \pm 0.1	6.3 \pm 0.5	6.2 \pm 0.8	1.3 \pm 0.3	36.5 \pm 1.6	26.6 \pm 1.0	1.3 \pm 0.1	0.5 \pm 0.1	6.5 \pm 0.5	6.3 \pm 0.9	1.8 \pm 0.3
	Diffusion Planner [‡] [43]	60.3 \pm 1.5	26.0 \pm 0.8	1.7 \pm 0.1	0.3 \pm 0.0	2.7 \pm 0.2	5.8 \pm 0.8	0.6 \pm 0.2	53.7 \pm 1.6	20.0 \pm 1.0	1.7 \pm 0.1	0.3 \pm 0.0	2.7 \pm 0.2	7.4 \pm 1.0	1.0 \pm 0.3
CoPark (Ours)	79.7 \pm 1.6	47.7 \pm 0.6	1.8 \pm 0.2	0.4 \pm 0.0	4.0 \pm 0.2	6.0 \pm 0.8	0.0 \pm 0.0	69.8 \pm 1.8	29.7 \pm 0.5	1.8 \pm 0.2	0.4 \pm 0.0	3.5 \pm 0.2	5.8 \pm 1.0	0.0 \pm 0.0	

Table 1: Zero-shot evaluation on DLP and DSC3D under both partner reaction modes (\pm std over 5 seeds; classical planners are deterministic). CoPark is trained on the custom layouts only, with no fine-tuning. Bold marks the best per column within each partner mode for SR, PErr, HErr, Coll, and Off. Path and Manv are diagnostic rather than ranked. [†]Diffusion Planner is trained directly on DLP and DSC3D human demonstrations, so it is in-distribution rather than zero-shot. [‡]HOPE uses a released checkpoint (no training seeds; not strictly zero-shot on DLP).

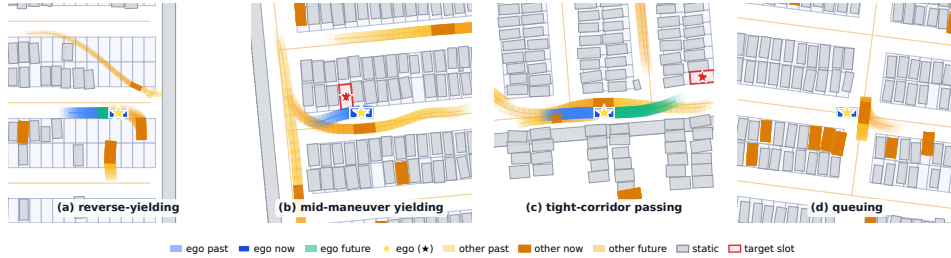


Figure 3: Emergent interaction behaviors of CoPark on held-out datasets. (a) Reverse-yielding: the ego backs out of an aisle to let an outgoing partner pass. (b) Mid-maneuver yielding: the ego pauses partway into its slot entry to give space to a crossing partner. (c) Tight-corridor passing: two agents traverse a narrow aisle within centimeter-scale clearance. (d) Queuing: agents form an orderly line behind a slow predecessor. The full token legend is shown at the bottom of the figure.

6.2 Main Results

Zero-shot Benchmark Results: CoPark leads on SR (84.7% / 79.7% / 75.8% / 69.8%) across two datasets under both partner reaction modes. Diffusion Planner (\sim 49%–60% in-distribution) and the large-scale RL recipes GigaFlow / CaRL (\sim 37%–51%) follow. GigaFlow leads on collisions (3.8% on DLP-Reactive, CoPark second at 4.1%), and CoPark is the only method reaching 0% off-road in all conditions. Classical planners lead on terminal precision (0.1 m PErr) via analytic geometry. Learning-based methods sit at 0.2 m–0.5 m. Manv separates the large-scale RL methods: CoPark’s \sim 1.7 maneuvers per episode match the human demonstration distribution (Appendix C.7) via reverse-in and re-tries, while GigaFlow / CaRL plateau on slots reachable in a single drive-in (Manv 1.1–1.3).

Failure Modes: Open-loop classical planners (RS, Hybrid A*+Stanley) lack partner awareness (57%–78% collision). MA-MPC’s closed-loop variant cuts collisions to 10%–20% but the partner-blind reference and the lack of multi-step reverse-in cap SR below 60%. HOPE’s single-agent DLP training plus open-loop RS terminal approach collapses on DSC3D transfer (8.4% / 6.5% SR). GigaFlow and CaRL do not discover multi-step reverse-in within budget, leaving terminal error stuck at 0.5 m. Diffusion Planner imitates human trajectories but does not internalize the closed-loop constraints arising when its own actions perturb partners (10.5% / 5.8% collision). CoPark’s failures concentrate in overcrowded aisles requiring centimeter-level accuracy. Per-source collision breakdowns (vehicle–vehicle vs. vehicle–static) for all methods are reported in Appendix C.8.

Emergent Multi-agent Behaviors: The four behaviors in Fig. 3 arise under self-play without behavior-specific rewards, and split by the phase in which interaction occurs. The first pair shows that the policy stays responsive to neighbors during the parking maneuver itself, not only during routing, which is the capability that distinguishes CoPark from prior parking pipelines. In reverse-yielding (a), the ego in its slot-entry maneuver detects an outgoing partner and yields longitudinally by backing

out, while the lateral channel stays anchored to the slot frame, jointly enabled by the asymmetric release and self-play training. Mid-maneuver yielding (b) relies on the longitudinal-only release: the residual pauses forward progress when a crossing partner enters its envelope, without abandoning the lateral reference that keeps slot alignment intact. The second pair shows the same responsiveness during normal navigation: in tight-corridor passing (c), self-play has driven the policy to enough precision for two agents to clear each other within centimeter-scale aisle clearance, while in queuing (d), self-play training has produced a yielding behavior behind a slow predecessor without any explicit coordination signal.

6.3 Ablation Study

We present a cumulative components analysis below. Eight further ablations and analyses (channel-wise prior-release sensitivity, scene-density curriculum, training-step scaling, success-criterion sensitivity, partner-observation noise, path/maneuver distribution, per-source collision breakdown, and self-play partner evaluation) are in Appendix C.

Starting from the GigaFlow self-play baseline (Tab. 2, DLP-Reactive row of Tab. 1), each row adds one CoPark module. The offline kinematic prior supplies a geometric reference that sharpens terminal precision and lifts SR by roughly 18 points, but the residual head now tracks a partner-blind plan, and collisions spike from 3.8% to 13.3%. Asymmetric reliance then releases the longitudinal channel while anchoring the lateral one, returning collisions to baseline (3.9%) and lifting SR another \sim ten points. Precision relaxes here as yielding pulls the policy off the prior, the residual error refinement then absorbs. Closed-loop refinement recovers precision and pushes SR to its 84.7% peak, with a small uptick in collisions from grazing neighbors mid-correction.

Variant	SR [%]	Coll [%]	PErr [m]
Vanilla GigaFlow [5]	50.8 \pm 1.7	3.8 \pm 0.7	0.5
+ Prior	68.7 \pm 1.7	13.3 \pm 1.2	0.2
+ Asym. reliance	78.3 \pm 1.5	3.9 \pm 0.7	0.5
+ Refinement (full CoPark)	84.7\pm1.4	4.1 \pm 0.7	0.4

Table 2: Cumulative components analysis on DLP-Reactive (\pm std over 5 seeds). Starting from the GigaFlow self-play baseline (DLP-Reactive row of Table 1), each row adds one CoPark module: offline kinematic prior, asymmetric channel-wise reliance, and closed-loop refinement.

7 Conclusion

We introduce reactive parking, the closed-loop multi-agent extension of automated parking, and propose CoPark, a self-play RL approach combining an offline kinematic prior, a residual policy with reactive yielding under partner threat, and a closed-loop refinement layer, all trained within a single parameter set under multi-agent self-play. CoPark substantially outperforms classical, imitation, and pure large-scale RL baselines on success rate under both partner reaction modes, with collision rates within a percentage point of the best large-scale RL baseline, and exhibits emergent interaction behaviors without behavior-specific rewards. Beyond the immediate result, CoPark instantiates a general principle: a geometric prior should be released to match a task’s anisotropic tolerance, anchored where tolerance is tight and relaxed where it is loose. We expect this principle to transfer to other multi-agent settings where strong geometric priors coexist with partner dynamics that cannot be pre-planned, provided the task’s precision tolerance aligns with distinct action channels.

8 Limitations

Compute constraints prevented scaling along orthogonal axes such as larger lot populations (the densest training tier was capped at 32 controlled agents per scene), longer training horizons, and broader hyperparameter sweeps. CoPark relies on an offline kinematic prior to attain terminal precision, and we have not yet explored a more end-to-end alternative that reaches the same accuracy without this external scaffold. Terminal precision is additionally bounded by the 91-way discrete action grid imposed by the PufferDrive simulator interface. A continuous-action substrate would further tighten PErr. Evaluation is sim-only within this submission’s budget. Real-world deployment would further require a passive safety layer given the tight accuracy tolerances of production-grade parking.

References

- [1] A. L. Samuel. Some studies in machine learning using the game of checkers. *IBM Journal of Research and Development*, 3(3):210–229, 1959.
- [2] T. Bansal, J. Pachocki, S. Sidor, I. Sutskever, and I. Mordatch. Emergent complexity via multi-agent competition. *arXiv preprint arXiv:1710.03748*, 2017.
- [3] D. Silver, J. Schrittwieser, K. Simonyan, I. Antonoglou, A. Huang, A. Guez, T. Hubert, L. Baker, M. Lai, A. Bolton, et al. Mastering the game of Go without human knowledge. *Nature*, 550(7676):354–359, 2017.
- [4] D. Silver, T. Hubert, J. Schrittwieser, I. Antonoglou, M. Lai, A. Guez, M. Lanctot, L. Sifre, D. Kumaran, T. Graepel, et al. A general reinforcement learning algorithm that masters chess, shogi, and Go through self-play. *Science*, 362(6419):1140–1144, 2018.
- [5] M. Cusumano-Towner, D. Hafner, A. Hertzberg, B. Huval, A. Petrenko, E. Vinitsky, E. Wijmans, T. Killian, S. Bowers, O. Sener, P. Krähenbühl, and V. Koltun. Robust autonomy emerges from self-play. In *Proceedings of the International Conference on Machine Learning (ICML)*, 2025.
- [6] S. Kazemkhani, A. Pandya, D. Cornelisse, B. Shacklett, and E. Vinitsky. GPUDrive: Data-driven, multi-agent driving simulation at 1 million FPS. In *Int. Conf. on Learning Representations*, 2025.
- [7] D. Cornelisse, A. Pandya, K. Joseph, J. Suárez, and E. Vinitsky. Building reliable sim driving agents by scaling self-play. *arXiv preprint arXiv:2502.14706*, 2025.
- [8] D. Cornelisse and E. Vinitsky. Human-compatible driving agents through data-regularized self-play reinforcement learning. *Reinforcement Learning Journal*, 5:2320–2344, 2024.
- [9] X. Xu, Y. Xie, R. Li, Y. Zhao, R. Song, and W. Zhang. Hierarchical reinforcement learning for autonomous parking based on kinematic constraints. In *IEEE International Conference on Robotics and Biomimetics (ROBIO)*, 2024.
- [10] R. Chai, D. Liu, T. Liu, A. Tsourdos, Y. Xia, and S. Chai. Deep learning-based trajectory planning and control for autonomous ground vehicle parking maneuver. *IEEE Transactions on Automation Science and Engineering*, 20(3):1633–1647, 2023.
- [11] D. Cornelisse*, S. Cheng*, P. Mandavilli, J. Hunt, K. Joseph, W. Doulazmi, V. Charraut, A. Gupta, J. Suarez, and E. Vinitsky. PufferDrive: A fast and friendly driving simulator for training and evaluating RL agents, 2025. URL <https://github.com/Emerge-Lab/PufferDrive>.
- [12] B. Jaeger, D. Dauner, J. Beißwenger, S. Gerstenecker, K. Chitta, and A. Geiger. CaRL: Learning scalable planning policies with simple rewards. In *Proc. of the Conf. on Robot Learning (CoRL)*, 2025.
- [13] W.-J. Chang, A. Rangesh, K. Joseph, M. Strong, M. Tomizuka, Y. Hu, and W. Zhan. SPACeR: Self-play anchoring with centralized reference models. In *Int. Conf. on Learning Representations*, 2026. Poster.
- [14] C. Zhang, S. Biswas, K. Wong, K. Fallah, L. Zhang, D. Chen, S. Casas, and R. Urtasun. Learning to drive via asymmetric self-play. In *European Conference on Computer Vision (ECCV)*, pages 149–168. Springer, 2024.
- [15] T. Hester, M. Vecerik, O. Pietquin, M. Lanctot, T. Schaul, B. Piot, D. Horgan, J. Quan, A. Sendonaris, I. Osband, G. Dulac-Arnold, J. Agapiou, J. Z. Leibo, and A. Gruslys. Deep Q-learning from demonstrations. In *AAAI Conf. on Artificial Intelligence*, pages 3223–3230, 2018.

- [16] F. Schmalstieg, D. Honerkamp, T. Welschehold, and A. Valada. Learning hierarchical interactive multi-object search for mobile manipulation. *IEEE Robotics and Automation Letters*, 8(12): 8549–8556, 2023.
- [17] A. L. Chandra, I. Nematollahi, C. Huang, T. Welschehold, W. Burgard, and A. Valada. Diwa: Diffusion policy adaptation with world models. *arXiv preprint arXiv:2508.03645*, 2025.
- [18] I. Nematollahi, E. Rosete-Beas, A. Röfer, T. Welschehold, A. Valada, and W. Burgard. Robot skill adaptation via soft actor-critic gaussian mixture models. In *International Conference on Robotics and Automation (ICRA)*, pages 8651–8657, 2022.
- [19] F. Schmalstieg, D. Honerkamp, T. Welschehold, and A. Valada. Learning long-horizon robot exploration strategies for multi-object search in continuous action spaces. In *The International Symposium of Robotics Research*, pages 52–66, 2022.
- [20] T. Johannink, S. Bahl, A. Nair, J. Luo, A. Kumar, M. Loskyll, J. Aparicio Ojea, E. Solowjow, and S. Levine. Residual reinforcement learning for robot control. In *IEEE Int. Conf. on Robotics and Automation*, pages 6023–6029, 2019.
- [21] T. Silver, K. R. Allen, J. B. Tenenbaum, and L. P. Kaelbling. Residual policy learning. *arXiv preprint arXiv:1812.06298*, 2018.
- [22] K. Rana, B. Talbot, M. Milford, and N. Sünderhauf. Residual reactive navigation: Combining classical and learned navigation strategies for deployment in unknown environments. In *IEEE Int. Conf. on Robotics and Automation*, pages 11493–11499, 2020.
- [23] M. Jiang, Y. Li, S. Zhang, S. Chen, C. Wang, and M. Yang. HOPE: A reinforcement learning-based hybrid policy path planner for diverse parking scenarios. *IEEE Transactions on Intelligent Transportation Systems*, 2025.
- [24] M. Jiang, Y. Li, J. Zhang, S. Zhang, and M. Yang. A diffusion-refined planner with reinforcement learning priors for confined-space parking. *arXiv preprint arXiv:2510.14000*, 2025.
- [25] J. Xie, Z. He, and Y. Zhu. A DRL based cooperative approach for parking space allocation in an automated valet parking system. *Applied Intelligence*, 53(5):5368–5387, 2023.
- [26] G. O. Boateng, H. Si, H. Xia, X. Guo, C. Chen, I. O. Agyemang, and N. Ansari. Automated valet parking and charging: A dynamic pricing and reservation-based framework leveraging multi-agent reinforcement learning. *IEEE Transactions on Intelligent Vehicles*, 10(2):1010–1029, 2025.
- [27] M. Kneissl, A. K. Madhusudhanan, A. Molin, H. Esen, and S. Hirche. A multi-vehicle control framework with application to automated valet parking. *IEEE Transactions on Intelligent Transportation Systems*, 22(9):5697–5707, 2021. doi:10.1109/TITS.2020.2990294.
- [28] X. Shen, Y. Choi, A. Wong, F. Borrelli, S. Moura, and S. Woo. Parking of connected automated vehicles: Vehicle control, parking assignment, and multi-agent simulation. *arXiv preprint arXiv:2402.14183*, 2024.
- [29] O. Tanner. Multi-agent car parking using reinforcement learning, 2022.
- [30] S. Chen, M. Wang, Y. Yang, and W. Song. Conflict-constrained multi-agent reinforcement learning method for parking trajectory planning. In *IEEE Int. Conf. on Robotics and Automation*, pages 9421–9427, 2023. doi:10.1109/ICRA48891.2023.10160698.
- [31] J. Wei, N. Vödösch, A. Rehr, C. Feist, and A. Valada. ParkDiffusion: Heterogeneous multi-agent multi-modal trajectory prediction for automated parking using diffusion models. In *IEEE/RSJ Int. Conf. on Intelligent Robots and Systems*, pages 8297–8304, 2025.

- [32] J. Wei, A. Rehr, C. Feist, and A. Valada. ParkDiffusion++: Ego intention conditioned joint multi-agent trajectory prediction for automated parking using diffusion models. In *IEEE Int. Conf. on Robotics and Automation*, 2026.
- [33] E. A. Hansen, D. S. Bernstein, and S. Zilberstein. Dynamic programming for partially observable stochastic games. In *AAAI Conf. on Artificial Intelligence*, volume 4, pages 709–715, 2004.
- [34] D. A. Dolgov, S. Thrun, M. Montemerlo, and J. Diebel. Path planning for autonomous vehicles in unknown semi-structured environments. *The International Journal of Robotics Research*, 29(5):485–501, 2010.
- [35] J. A. Reeds and L. A. Shepp. Optimal paths for a car that goes both forwards and backwards. *Pacific Journal of Mathematics*, 145(2):367–393, 1990.
- [36] G. M. Hoffmann, C. J. Tomlin, M. Montemerlo, and S. Thrun. Autonomous automobile trajectory tracking for off-road driving: Controller design, experimental validation and racing. In *American Control Conference (ACC)*, pages 2296–2301, 2007.
- [37] J. Schulman, F. Wolski, P. Dhariwal, A. Radford, and O. Klimov. Proximal policy optimization algorithms. *arXiv preprint arXiv:1707.06347*, 2017.
- [38] L. Espeholt, H. Soyer, R. Munos, K. Simonyan, V. Mnih, T. Ward, Y. Doron, V. Firoiu, T. Harley, I. Dunning, S. Legg, and K. Kavukcuoglu. IMPALA: Scalable distributed deep-RL with importance weighted actor-learner architectures. In *Proceedings of the International Conference on Machine Learning (ICML)*, 2018.
- [39] J. Suarez. PufferLib: Making reinforcement learning libraries and environments play nice. *arXiv preprint arXiv:2406.12905*, 2024.
- [40] X. Shen, M. Lacayo, N. Guggilla, and F. Borrelli. ParkPredict+: Multimodal intent and motion prediction for vehicles in parking lots with CNN and transformer. In *IEEE Int. Conf. on Intelligent Transportation Systems*, pages 3999–4004, 2022. doi:10.1109/ITSC55140.2022.9922162.
- [41] O. Dhaouadi, J. Meier, L. Wahl, J. Kaiser, L. Scalerandi, N. Wandelburg, Z. Zhou, N. Berinpanathan, H. Banzhaf, and D. Cremers. Highly accurate and diverse traffic data: The Deep-Scenario open 3D dataset. In *IEEE Intelligent Vehicles Symposium*, pages 377–384, 2025. doi:10.1109/IV64158.2025.11097484.
- [42] M. Treiber, A. Hennecke, and D. Helbing. Congested traffic states in empirical observations and microscopic simulations. *Physical Review E*, 62(2):1805–1824, 2000.
- [43] Y. Zheng, R. Liang, K. Zheng, J. Zheng, L. Mao, J. Li, W. Gu, R. Ai, S. E. Li, X. Zhan, and J. Liu. Diffusion-based planning for autonomous driving with flexible guidance. In *Int. Conf. on Learning Representations*, 2025.

CoPark: Learning Reactive Parking via Self-Play

Appendix

A Training Details

This section collects the implementation details supporting the training setup of Sec. 6.1. We describe the parking-lot layouts and scene sampling pipeline (Appendix A.1), the observation interface and policy architecture (Appendix A.2), the reward composition with per-agent conditioning (Appendix A.3), and the optimization recipe (Appendix A.4). A visualization of the observation features and the resulting policy distribution on a representative episode closes the section (Appendix A.5).

A.1 Training Maps and Scene Construction

Training uses six custom parking-lot layouts, all normalized into a common clean-map representation that declares the drivable region, slot poses with footprints, a directed lane graph, and static-obstacle polygons. DLP [40] and DSC3D [41] are converted into the same representation for zero-shot evaluation (Appendix B.1). The six layouts span a range of parking-lot footprints and aisle topologies, providing the layout diversity that CoPark’s policy generalizes across before zero-shot transfer.

Each scene samples a static-occupancy fraction and a controlled-agent count from a three-tier stratification with occupancies 0.25, 0.50, and 0.75, up to 32 controlled vehicles per scene, and the densest tier weighted at 50%. Static parked vehicles are placed uniformly at random in unoccupied slots and merged into the scene’s road_{edge} geometry, a workaround required by the maximum-controlled-agent cap of the PufferDrive simulator. A source tag is retained on every merged static vehicle so that vehicle–vehicle, vehicle–static, and off-road terminal events remain distinguishable in downstream analysis (Appendix C.8). For each controlled agent, an initial pose and an injective slot assignment are drawn offline under a kinematic-reachability check and held fixed throughout the episode.

A.2 Observation Space and Policy Architecture

The policy is a single parameter-sharing categorical actor $\pi_\theta(a | s)$ over the 91-way discrete action grid (7 acceleration levels by 13 steering angles), with a shared backbone fusing five feature blocks. The ego block carries the agent’s kinematic state. The partner block carries the relative state of the $K = 8$ nearest neighbors as oriented bounding boxes in ego frame; $K = 8$ covers the 99th percentile of nearby-vehicle counts within the observation range across training scenes, and larger values of K provided no measurable improvement in pilot studies. The road block carries polyline tokens for lane centerlines and parking-lot boundaries, sampled around the ego in ego frame under per-class token budgets. The reward-conditioning block carries the per-agent weights (w_g, w_c) defined in Appendix A.3. The tail block carries the 10-dimensional normalized scalar summary of the closing-threat and static-clearance signals, the signed slot-frame errors, the Stanley reference command, the teacher cross-track and heading errors, and the ego signed velocity.

The Stanley reference enters the actor as a channel-wise log-prior added to the policy logits (Eq. 3), with the reliance scalars contracting along the saturated threat signal $\rho(s)$ (Eq. 7). The residual logit head $z_\theta(s, a)$ is bounded so that the prior pull retains effect when $\rho(s) \rightarrow 0$. The Stanley controller writes nothing to the simulator; its action enters the policy only through the log-prior channel. The slot-frame errors and the Stanley command are zeroed during the navigation phase and become informative only after the agent transitions to the parking-maneuver phase, so that the phase-conditional prior of Eq. 3 fires only when geometrically meaningful.

A.3 Reward Composition and Per-Agent Conditioning

The per-agent reward decomposes into four groups (Table 3). A sparse terminal group fires only on episode-ending events. A phase-independent dense safety group is active throughout the episode. Two phase-dependent dense shaping groups take effect during navigation and during the parking maneuver respectively. Contact is terminal and removes the agent from the rollout, so no in-contact dense penalty is needed.

Group	Term	When active
Sparse terminal	Success bonus	on success (Eq. 1)
	Terminal collision penalty	on V-V or V-Stat contact
	Navigation→Maneuver handoff bonus	on entering maneuver phase
Dense safety (both phases)	Closing-threat penalty $-\beta_{\text{dyn}} \cdot \text{threat}_i$	continuous in threat_i (Eq. 4)
	Static-clearance penalty	if $\text{ego} < \text{clearance margin to static edge}$
Navigation shaping	Lane-graph progress	per step along \mathcal{G}
	Subgoal bonus	on reaching each $g_{i,k}$
	Triangular speed-target reward	per step under target speed band
Maneuver shaping	Arc-along-plan progress	per step along τ_i
	Threat-modulated imitation $r_{i,t}^{\text{imit}}$ (Eq. 5)	scaled by $(1 - \rho(s)) w_{\text{trust}}(s)$
	Refinement reward $r_{i,t}^{\text{ref}}$ (Eq. 8)	during closed-loop refinement

Table 3: Per-agent reward decomposition. Numerical values of the weights ($\beta_{\text{dyn}}, \alpha_{\text{imit}}, \beta_{\text{red}}, \beta_{\text{hold}}$) and of the prior-modulation hyperparameters (Eqs. 6, 7) are listed in Table 4.

The numerical values of the method-side hyperparameters introduced in Sec. 4 are collected in Table 4. The static-clearance gate slope β_{stat} is set steep so that $\sigma(\beta_{\text{stat}}(d_{\text{stat}} - d_0))$ approximates a hard step at d_0 .

Symbol	Description	Value
Threat signal and prior modulation (Eqs. 4, 7)		
d_{decay}	threat range decay constant	4.5 m
τ_{ρ}	threat squash scale (ρ saturation)	1.0 m/s
$\alpha_{\text{min}}, \alpha_{\text{max}}$	reliance scalar range	1.0, 4.0
$\kappa^{\text{acc}}, \kappa^{\text{steer}}$	channel-wise release rates	0.95, 0.40
Trust-weight components (Eq. 6)		
σ_{ct}	cross-track suppression scale	1.5 m
β_{stat}	static-clearance gate slope	20 m^{-1}
d_0	static-clearance threshold	0.35 m
Reward weights (Eqs. 5, 8)		
α_{imit}	threat-modulated imitation weight	0.20
σ_{imit}	imitation command-match scale	0.50
β_{dyn}	dynamic threat penalty weight	0.10
β_{red}	refinement directed-gradient gain	0.25
β_{hold}	refinement hold bonus	0.08
η	refinement tanh saturation scale	0.10 m

Table 4: Numerical values of the method-side hyperparameters of Sec. 4.

Each agent additionally receives a pair of conditioning weights (w_g, w_c) that scale the goal-related and collision-related reward components respectively, following the recipe of GigaFlow [5]. The weights are sampled per agent at episode start from $w_g \sim \mathcal{U}[0.5, 2.0]$ and $w_c \sim \mathcal{U}[0.5, 3.0]$, so that a single policy spans a continuum of operational styles from cautious-and-precise to aggressive-and-fast within the same parameter set. The same range is later swept at inference time in Appendix C.9 to demonstrate operating-point control on a single trained checkpoint.

A.4 Optimization Recipe and Training Hyperparameters

Training uses the PPO [37] variant in PufferLib [39] with V-trace [38] advantages under parameter sharing, for 4×10^9 environment steps on 2 NVIDIA RTX A6000 GPUs, sustaining approximately 120k simulator steps per second at episode length 400. The three-tier scene-density curriculum of Appendix A.1 schedules occupancies 0.25, 0.50, and 0.75 with the densest tier sampled at 50%, exposing the policy to progressively denser interactions over the course of training. The same parameter set θ is shared across both phases, all agents, and all episodes; phase information enters only through the phase indicator $\phi_{i,t}$ in the observation and through the phase-conditional prior of Eq. 3. Completed agents are removed from the rollout on termination, so the active-agent count varies during an episode.

A.5 Observation and Policy-Distribution Visualization

To make concrete what CoPark’s policy reads and writes, Fig. 4 visualizes a single representative training episode on one of the custom parking-lot layouts at three phase-defining instants: free-roaming navigation, the start of the parking maneuver near the preparation pose, and the late maneuver as the ego closes onto its slot. Every row shares the same five-panel layout, described as follows.

- **Ground truth (left).** Bird’s-eye view of the lot. The ego is red, static parked vehicles slate, other controlled agents blue, the assigned target slot a yellow dashed rectangle, the navigation-route endpoint (preparation pose p_i^{prep}) a yellow star, and the Hybrid A* plan with its Stanley reference appear as the yellow line with circle waypoint markers.
- **Partner OBBs (top-mid).** The partner oriented bounding boxes the policy actually sees in ego frame, after K -nearest-neighbors cropping ($K = 8$). The annotation n/N at the panel header reports the n partners retained within the observation range out of the N total present in the scene, and the dashed rings indicate the observation range.
- **Map tokens (top-right).** The polyline tokens (lane centerlines and parking-lot boundaries) sampled around the ego in ego frame, with the per-class token budget actually used (LANE/BOUND counts).
- **Core tail scalars (bottom-mid).** The 10-dimensional normalized scalar tail of the observation: the closing-threat and static-clearance scalars, the signed slot-frame errors (slot_long, slot_lat, slot_head), the Stanley target (stanley_a, stanley_s), the teacher cross-track and heading errors, and the ego signed velocity.
- **Policy distribution $\pi_\theta(a | s)$ (bottom-right).** The full categorical distribution over the 7×13 acceleration–steering action grid, with the sampled action outlined in red and its probability p printed at the panel header.

Three structural properties of the observation are immediately visible from the comparison. (i) The phase one-hot switches cleanly from NAV_ROUTE (top) to PARK_EXECUTE (middle, bottom). The slot-frame errors and the Stanley target are exactly zero during navigation and become informative only once the parking-maneuver phase starts, exactly as required by the phase-conditional prior of Eq. 3 and the threat-modulated imitation reward of Eq. 5. (ii) Partner density falls from 4/31 in the open navigation phase to 1/31 inside the dense aisle while map-token counts stay roughly constant (LANE 33–49, BOUND 10–20), confirming that the cropping budget is exercised by partners rather than map geometry. (iii) The policy distribution evolves with the phase. It is broad over the action grid during navigation (sampled-action probability $p = 0.02$, reflecting genuine in-traffic uncertainty), tightens to a localized mode at maneuver onset ($p = 0.18$), and sharpens further into a near-deterministic forward step at late maneuver ($p = 0.35$). The progression shows how the residual head retains exploratory entropy while the prior is dormant and concentrates onto the prior-anchored geometric reference as the slot frame becomes informative.

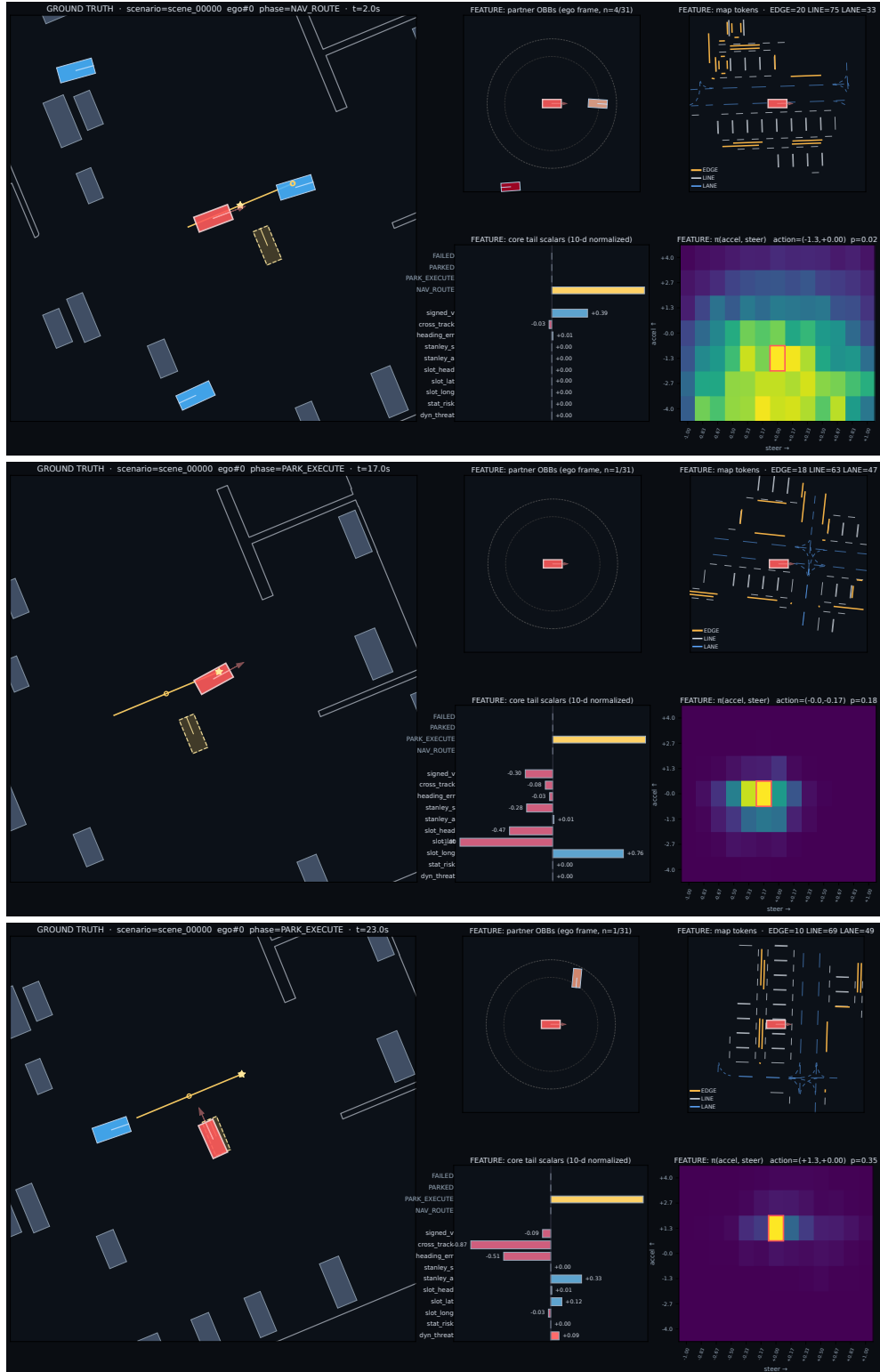


Figure 4: Policy observation and action distribution at three phases of a representative training episode on a custom parking-lot layout (same agent, same scene). The top row at $t = 2.0$ s shows phase NAV_ROUTE, free-roaming navigation with 4/31 partners in range. The middle row at $t = 17.0$ s shows phase PARK_EXECUTE at maneuver onset near the preparation pose, with large slot-frame offsets (slot_long = +0.76, slot_lat = -1.00). The bottom row at $t = 23.0$ s shows phase PARK_EXECUTE late maneuver, with the ego nearly aligned to its slot (slot_long = -0.03, slot_lat = +0.12). Each row uses the same five-panel layout described in the text.

B Benchmark Implementation Details

This section provides the implementation details that ensure all methods are evaluated under identical conditions. We describe the source datasets and episode construction (Appendix B.1), the success criterion and tolerances (Appendix B.2), the three partner modes used in evaluation (Appendix B.3), the evaluation harness and shared action interface (Appendix B.4), and the adaptation procedure for each baseline (Appendix B.5).

B.1 Datasets and Episode Construction

We integrate the Dragon Lake Parking dataset (DLP) [40] and the DeepScenario Open 3D dataset (DSC3D) [41] into the PufferDrive [11] simulator under the formulation of Sec. 3. Both datasets are converted into the same clean-map representation used at training (Appendix A.1), comprising a drivable region, slot poses with footprints, a directed lane graph, and static-obstacle polygons. Every source-data parking trajectory yields one ego-episode in which the ego is the original parking driver and the assigned slot is its final logged pose. Non-ego agents present in the source data are converted into scripted partners (Appendix B.3). The two datasets differ in scene structure. DSC3D mixes through-road segments with parking-garage areas, whereas CoPark’s training layouts are pure parking-garage environments, so the lane-graph topology DSC3D presents at evaluation departs from the structure seen during self-play. This structural gap underpins the zero-shot transfer gap analyzed in Appendix C.3.

B.2 Success Criterion and Tolerances

An episode ends in success, collision, off-road, refinement timeout (when the budget $K_{\text{ref}}^{\text{max}}$ is exhausted), or horizon timeout. Success requires Eq. 1 to hold for K_s consecutive steps in the slot-aligned frame. Numerical tolerances and horizons are listed in Table 5. The position criterion is the Euclidean slot-frame distance $\|e_{i,t}^{\text{slot}}\|_2 \leq \Delta_d$, so the reported PErr in Table 1 and the success gate share a single geometric notion. The 10° heading tolerance with modulo- π wrapping accepts both forward-in and reverse-in slot entries.

Table 5: Evaluation parameters of the PufferDrive reactive-parking benchmark.

Parameter	Value
Simulator step size	0.1 s (10 Hz)
Training / evaluation horizon	400 / 1,800 steps
Refinement budget $K_{\text{ref}}^{\text{max}}$	80 steps
Success tolerance, position Δ_d	0.8 m (Euclidean distance to slot center)
Success tolerance, heading Δ_ψ	0.1745 rad $\approx 10^\circ$ (modulo π)
Success tolerance, speed Δ_v	0.35 m/s
Required hold duration K_s	5 consecutive steps
Controlled-agent dimensions (L \times W, wheelbase)	3.2×1.4 m, 2.1 m

B.3 Partner Modes

Following the closed-loop protocol of GigaFlow [5], each method controls a single ego in every episode while all non-ego partners advance under one of three scripted modes. The reactive mode advances each non-ego partner along its logged route using IDM [42], with the longitudinal command decelerating in response to the ego’s proximity. The non-reactive mode replays each non-ego partner’s logged trajectory regardless of the ego’s behavior, producing the harder collision-avoidance condition because partners do not yield. The self-play mode advances every non-ego partner under the same CoPark policy as the ego, with each partner pursuing its own assigned slot. The reactive and non-reactive modes form the headline two partner-mode blocks of Table 1. The self-play mode is reported separately in Appendix C.5.

B.4 Evaluation Harness and Action Interface

At every 0.1 s step the harness collects the joint state, constructs the ego observation, and queries the method under test for one of the 91 discrete acceleration–steering primitives. The 7×13 grid is mandated by the PufferDrive simulator’s action interface and sets an inherent floor on terminal precision across all methods; CoPark’s sub-meter PErr in Table 1 operates near this discretization limit. All baselines that natively produce continuous commands are projected onto the same grid by nearest-grid-cell assignment at each step. The Stanley-tracked commands from classical planners, the MPC commands of MA-MPC, HOPE’s policy outputs, and Diffusion Planner’s sampled actions are all discretized this way before being applied to the simulator. GigaFlow and CaRL already operate over the same discrete grid in our reimplementation. The shared action interface and shared contact model ensure that performance differences in Table 1 reflect policy quality rather than action-space mismatch.

B.5 Baseline Adaptations

Classical planners. RS [35] re-plans a Reeds–Shepp curve from the agent’s current pose to its assigned slot at every step. Hybrid A* [34] uses the same plan library that CoPark uses offline, but invoked online and tracked open-loop by Stanley control without the learned residual.

MA-MPC. Each ego runs a receding-horizon predictive controller over the same Hybrid A* reference path used in the Hybrid A*+Stanley row, with dynamic-obstacle constraints constructed from observed partner positions and a constant-velocity prediction over the horizon. The continuous MPC command is projected onto the 91-way action grid (Appendix B.4) before being applied. The framework follows the multi-vehicle MPC recipe of [27], adapted from V2I-coordinated to decentralized per-agent execution.

HOPE. HOPE [23] couples a learned RL policy with rule-based Reeds–Shepp curves via action masking. We reuse the released checkpoint adapted to the PufferDrive observation format. Since HOPE is trained on parking scenes derived from DLP layouts, its evaluation on DLP is not strictly zero-shot, while on DSC3D it is.

GigaFlow and CaRL. GigaFlow [5] and CaRL [12] are two large-scale RL recipes trained on the same six maps and same compute budget as CoPark, but without the CoPark components. The two differ in reward complexity. GigaFlow uses a richer per-agent reward continuum, while CaRL uses a deliberately simple reward. Both plateau on success rate well below CoPark in the dense low-speed parking domain.

Diffusion Planner. Diffusion Planner [43] is trained in its standard imitation regime directly on DLP and DSC3D human demonstrations using fixed-time-budget trajectory windows, with the original sampler, guidance, and projection pipeline retained. This baseline sees the real evaluation datasets at training time, while CoPark does not. CoPark nonetheless outperforms it across all four (dataset, partner-mode) configurations.

C Ablations and Extended Analyses

This section complements the cumulative components analysis of Sec. 6.3 with deeper studies organized into four groups. Two method-design ablations isolate the channel-wise prior-release asymmetry (Appendix C.1) and the scene-density curriculum (Appendix C.2). A training-dynamics study reports the convergence behavior of zero-shot SR over the full training budget (Appendix C.3). Three robustness analyses probe success-criterion sensitivity (Appendix C.4), the self-play partner mode (Appendix C.5), and partner-observation noise (Appendix C.6). Two behavioral analyses characterize trajectory naturalism against human demonstrations (Appendix C.7) and the per-source

collision breakdown across methods (Appendix C.8). A final operating-point analysis demonstrates inference-time control through per-agent reward conditioning (Appendix C.9).

C.1 Channel-Wise Prior-Release Sensitivity

The reliance scalars of Eq. 7 contract along $\rho(s)$ at independently tunable rates κ^{acc} and κ^{steer} per channel. Table 6 sweeps the two-dimensional configuration space at $\kappa \in \{0.40, 0.70, 0.95\}$ per channel on DLP-Reactive, yielding nine configurations grouped into a symmetric diagonal, a reverse-asymmetric block ($\kappa^{\text{steer}} > \kappa^{\text{acc}}$), and a correct-asymmetric block ($\kappa^{\text{acc}} > \kappa^{\text{steer}}$). Collisions are split into vehicle–vehicle (V–V) and vehicle–static (V–Stat) contacts to expose the underlying trade-off.

$(\kappa^{\text{acc}}, \kappa^{\text{steer}})$	SR [%]	Coll [%]	V–V [%]	V–Stat [%]
<i>Symmetric</i> ($\kappa^{\text{acc}} = \kappa^{\text{steer}}$)				
(0.40, 0.40)	70.5 \pm 1.7	11.8 \pm 1.2	8.4 \pm 1.0	3.4 \pm 0.6
(0.70, 0.70)	76.3 \pm 1.5	8.9 \pm 1.0	5.2 \pm 0.8	3.7 \pm 0.6
(0.95, 0.95)	78.2 \pm 1.6	7.6 \pm 1.0	2.1 \pm 0.5	5.5 \pm 0.8
<i>Reverse asymmetric</i> ($\kappa^{\text{steer}} > \kappa^{\text{acc}}$)				
(0.40, 0.70)	69.3 \pm 1.7	11.4 \pm 1.2	7.5 \pm 0.9	3.9 \pm 0.6
(0.40, 0.95)	66.8 \pm 1.8	14.4 \pm 1.4	8.6 \pm 1.1	5.8 \pm 0.8
(0.70, 0.95)	73.5 \pm 1.6	9.7 \pm 1.1	4.6 \pm 0.7	5.1 \pm 0.7
<i>Correct asymmetric</i> ($\kappa^{\text{acc}} > \kappa^{\text{steer}}$)				
(0.70, 0.40)	80.5 \pm 1.5	6.5 \pm 0.9	4.2 \pm 0.7	2.3 \pm 0.5
(0.95, 0.70)	81.4 \pm 1.5	6.4 \pm 0.9	2.6 \pm 0.6	3.8 \pm 0.6
(0.95, 0.40) (default)	84.7\pm1.4	4.1\pm0.7	2.4\pm0.5	1.7\pm0.4

Table 6: Two-dimensional sweep of the channel-wise prior-release rates ($\kappa^{\text{acc}}, \kappa^{\text{steer}}$) on DLP-Reactive (\pm std over 5 seeds), evaluated at $\kappa \in \{0.40, 0.70, 0.95\}$ per channel. Rows are grouped into symmetric, reverse-asymmetric ($\kappa^{\text{steer}} > \kappa^{\text{acc}}$), and correct-asymmetric ($\kappa^{\text{acc}} > \kappa^{\text{steer}}$) blocks. Collisions are split into vehicle–vehicle (V–V) and vehicle–static (V–Stat) contacts. Bold marks the configuration used throughout the rest of the paper.

The sweep separates release magnitude from release direction. Along the symmetric diagonal, V–V contacts fall monotonically from 8.4% to 2.1% as the release rate rises (more longitudinal yielding) while V–Stat contacts climb from 3.4% to 5.5% (more lateral drift off the slot reference), and SR plateaus in the 70–78% band. In the reverse-asymmetric block, V–V stays in the range 4.6–8.6% because the longitudinal anchor blocks yielding, while V–Stat rises to 3.9–5.8% as the unanchored lateral channel drifts off the slot reference. SR in this block collapses to 66.8% at the extreme (0.40, 0.95), the lowest of the nine configurations and 11.4 points below the best symmetric configuration. The correct-asymmetric block breaks the trade-off in both directions simultaneously, with every entry beating every symmetric and every reverse-asymmetric point on SR. The default (0.95, 0.40) reaches V–V 2.4%, essentially matching the best longitudinal-yielding symmetric configuration (symm-high at 2.1%), while V–Stat drops to 1.7%, below all other configurations. SR climbs to 84.7%, exceeding every other configuration by at least 3.3 points (over (0.95, 0.70)) and by up to 17.9 points (over (0.40, 0.95)). The direction of the asymmetry, not the release magnitude, is therefore the operative design choice. Releasing the longitudinal channel while anchoring the lateral one enables yielding without sacrificing the slot-frame reference, whereas the reverse pairing degrades both metrics simultaneously.

C.2 Scene-Density Curriculum Ablation

The scene-density curriculum of Appendix A.1 stratifies training over three occupancy tiers (0.25, 0.50, 0.75) with the densest tier weighted at 50%. Replacing this stratified schedule with a uniform mixed-density distribution from the start, where occupancy is sampled with equal weight across the three tiers throughout training, drops final SR on DLP-Reactive by approximately 14.5 points (from 84.7% to roughly 70.2%). The mechanism is that the policy is overwhelmed by dense partners before it has time to learn navigation, leaving incomplete recovery within the same compute budget. The asymmetric weighting in the stratified schedule is therefore necessary for the policy to acquire navigation competence before being exposed to the densest interaction regime.

C.3 Training-Step Scaling

Figure 5 reports the training-step scaling of zero-shot SR on DLP and DSC3D, alongside the training-set reference curve. Both zero-shot curves and the reference rise steeply through the first 1×10^9 training steps, reaching roughly 77% of the final SR, before plateauing in the last 1×10^9 steps with gains below 0.5%. The roughly 17-point gap from the training set to DSC3D traces to the scene-structure difference quantified in Appendix B.1, where through-road segments mix with garage areas unlike the pure-garage training layouts. DLP, a pure parking-garage dataset structurally closer to the training layouts, shows a correspondingly smaller 8-point gap. The monotonic rise of the zero-shot curves with the training reference, rather than a divergence, indicates that the policy learns generalizable structure from multi-agent self-play rather than memorizing training layouts.

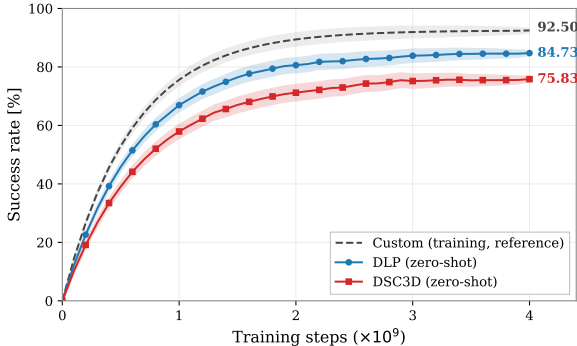


Figure 5: Zero-shot success rate on DLP and DSC3D as a function of training step (± 1 std across 5 training seeds), alongside the training-set reference curve. Zero-shot SR rises monotonically and tracks the reference throughout the climb, indicating generalizable structure learned from multi-agent self-play rather than memorization of training layouts.

C.4 Success-Criterion Sensitivity

The headline tolerance $(\Delta_d, \Delta_\psi) = (0.8 \text{ m}, 10^\circ)$ in Table 5 reflects practical parking-slot fit-in clearance. Table 7 examines how CoPark’s SR responds to progressively tighter criteria. All other evaluation settings and the trained checkpoint are unchanged; only the success gate is reapplied to the same rollouts.

Tolerance (Δ_d, Δ_ψ)	DLP-Reactive SR [%]	DSC3D-Reactive SR [%]
$(0.8 \text{ m}, 10^\circ)$ (default)	84.7 ± 1.4	75.8 ± 1.7
$(0.6 \text{ m}, 8^\circ)$	80.5 ± 1.5	71.8 ± 1.7
$(0.4 \text{ m}, 6^\circ)$	62.3 ± 1.8	54.2 ± 1.9
$(0.2 \text{ m}, 4^\circ)$	28.4 ± 2.1	23.6 ± 2.2

Table 7: CoPark’s SR under progressively tighter success criteria (\pm std over 5 training seeds). The same trained checkpoint is reused; only the post-rollout success gate is varied.

Degradation is gentle from $(0.8, 10^\circ)$ to $(0.6, 8^\circ)$ where the criterion still sits above the mean terminal error of Table 1 (PErr = 0.4 m, HErr = 3.9°). The drop steepens at $(0.4, 6^\circ)$ where the criterion bisects the terminal-error distribution, and at $(0.2, 4^\circ)$ where the criterion approaches the discretization limit of the 91-way action grid on which the refinement layer operates. Classical planners, which achieve decimeter-level PErr (Table 1), do not benefit from tighter criteria in practice because their absolute SR remains bounded by open-loop collisions.

C.5 Self-Play Partner Evaluation

The reactive and non-reactive partner modes of Appendix B.3 bracket the partner-difficulty spectrum, but neither uses a partner that is itself an active multi-agent planner. We re-evaluate the same trained checkpoint on DLP with all non-ego partners advanced by the same CoPark policy, so that every vehicle in the lot pursues its own assigned slot under the same residual-prior controller. The result (Table 8) sits between the two scripted partner modes on SR and below both on collision rate.

Partner mode (DLP)	SR [%]	PErr [m]	HErr [°]	Coll [%]
IDM (reactive, default)	84.7 \pm 1.4	0.4 \pm 0.0	3.9 \pm 0.2	4.1 \pm 0.7
Log replay (non-reactive)	79.7 \pm 1.6	0.4 \pm 0.0	4.0 \pm 0.2	6.0 \pm 0.8
CoPark (self-play)	80.4 \pm 1.6	0.4 \pm 0.0	4.0 \pm 0.2	3.6 \pm 0.6

Table 8: Evaluation on DLP with three partner modes (\pm std over 5 training seeds). The CoPark-partner row uses the same trained checkpoint as the ego on every non-ego vehicle.

SR drops 4.3 points relative to IDM-reactive because CoPark partners actively pursue their own slots and therefore compete for aisle space that IDM never claims, making genuine conflict cases more frequent. The same mechanism, however, makes them mutually responsive: collisions fall from 4.1% (IDM) to 3.6% thanks to two-sided yielding, lower than either scripted mode. Terminal precision is unchanged because the closed-loop refinement layer operates in the slot-aligned frame, where partner identity does not enter. The result confirms that CoPark’s self-play training transfers to interactions with learned partners, not only to scripted ones, while still leaving headroom above all baselines in Table 1.

C.6 Robustness to Partner-Observation Noise

The policy is trained on clean simulator observations. To probe sensitivity to the partner-perception inaccuracies expected at deployment, we re-evaluate the same trained checkpoint with isotropic Gaussian noise added to every partner oriented bounding box at inference time, perturbing both position (independently per ego-frame axis) and heading. Three noise levels span a representative range from a high-quality LiDAR detection regime to a stressed sim-to-real condition, and the clean configuration is included as the reference. The training procedure and trained weights are unchanged across rows.

Noise level ($\sigma_{\text{pos}}, \sigma_{\text{head}}$)	SR [%]	Coll [%]	V-V [%]	V-Stat [%]
None (clean, default)	84.7 \pm 1.4	4.1 \pm 0.7	2.4 \pm 0.5	1.7 \pm 0.4
Low (0.10 m, 2°)	83.5 \pm 1.4	4.4 \pm 0.7	2.7 \pm 0.5	1.7 \pm 0.4
Medium (0.25 m, 5°)	81.2 \pm 1.5	5.3 \pm 0.8	3.5 \pm 0.6	1.8 \pm 0.5
High (0.50 m, 10°)	75.6 \pm 1.7	7.8 \pm 0.9	5.6 \pm 0.7	2.2 \pm 0.5

Table 9: Robustness of CoPark to Gaussian noise injected into partner pose observations at inference time on DLP-Reactive (\pm std over 5 seeds). The same trained checkpoint is evaluated across all rows; the training procedure and the static map remain unperturbed.

The degradation is graceful and asymmetric across the two collision channels. SR drops by 1.2, 3.5, and 9.1 points at low, medium, and high noise respectively, retaining a lead over the strongest baseline (MA-MPC at 58.5% on DLP-Reactive) at every noise level. V-V collisions rise from 2.4% to 5.6% as the noise level climbs, since the threat signal of Eq. 4 reads directly from perturbed partner pose and the longitudinal yielding decision becomes correspondingly less precise. V-Stat collisions are nearly invariant across the four conditions (1.7–2.2%), because the lateral channel is anchored to the offline plan derived from static-map geometry, which the noise does not perturb. The channel-asymmetric prior release of Eq. 7 therefore confers an additional robustness property by construction. The lateral slot-frame alignment is shielded from partner-perception noise even though the longitudinal channel relies on it.

C.7 Path Length and Maneuver Distribution vs. Human Demonstrations

Sec. 6.2 reports that self-play methods produce the longest paths, consistent with safer navigation toward more distant goals, while CoPark’s maneuver count further matches the human demonstration distribution thanks to learned reverse-in. Table 10 quantifies this by comparing CoPark, two strongest learning baselines, and the logged human-demonstration distributions on the same DLP and DSC3D test sets.

Dataset	Source	Path [m]	Manv
DLP	Human demonstrations	46.2 \pm 14.3	1.8 \pm 0.7
	CoPark (Ours)	47.6 \pm 11.8	1.7 \pm 0.5
	Diffusion Planner [43]	25.8 \pm 8.0	1.7 \pm 0.4
	GigaFlow [5]	43.8 \pm 11.0	1.1 \pm 0.3
DSC3D	Human demonstrations	28.9 \pm 9.6	1.7 \pm 0.6
	CoPark (Ours)	29.6 \pm 7.6	1.7 \pm 0.5
	Diffusion Planner [43]	19.8 \pm 6.0	1.7 \pm 0.4
	GigaFlow [5]	27.5 \pm 7.5	1.2 \pm 0.3

Table 10: Per-episode path-length and maneuver-count distributions (mean \pm std over episodes), for the human demonstrations on each dataset and the three strongest closed-loop methods on the same evaluation set.

CoPark’s distributions sit within one standard deviation of the human demonstrations on both datasets ($\Delta\text{Path} \leq 1.4$ m, $\Delta\text{Manv} \leq 0.1$), and GigaFlow’s path length is also comparable, reflecting that self-play yields long-horizon navigation toward distant goals. Diffusion Planner systematically takes shorter paths because its imitation target is a fixed-time-budget trajectory window that under-represents the full navigation chain. The two self-play methods diverge on maneuver count: GigaFlow uses markedly fewer maneuvers than CoPark or human drivers because pure self-play discovers only slots reachable by a single drive-in arc, while CoPark’s learned reverse-in matches the human distribution. Path-length alignment is therefore not an artifact of inefficient routing but a sign that CoPark engages the full distribution of human-realistic parking attempts, including longer-haul and multi-step ones.

C.8 Collision Breakdown by Source Channel

The simulator wrapper retains a source tag on every contact event (Appendix A.1), allowing the headline collision rate to be decomposed into vehicle–vehicle (V–V) and vehicle–static (V–Stat) channels (Table 11). CoPark’s V–V and V–Stat split is roughly balanced (2.4% and 1.7%), confirming the design intent of the asymmetric prior release (Sec. 4.3) that yielding does not trade vehicle–vehicle risk for static-collision risk. Imitation baselines without that mechanism (HOPE, Diffusion Planner) are dominated by V–V failures.

Method	Coll [%]	V–V [%]	V–Stat [%]
HOPE [†] [23]	38.2	29.6	8.6
GigaFlow [5]	3.8 \pm 0.7	2.5 \pm 0.5	1.3 \pm 0.4
CaRL [12]	4.5 \pm 0.7	3.0 \pm 0.6	1.5 \pm 0.4
Diffusion Planner [43]	10.5 \pm 1.0	7.4 \pm 0.8	3.1 \pm 0.5
CoPark (Ours)	4.1 \pm 0.7	2.4 \pm 0.5	1.7 \pm 0.4

Table 11: Per-channel collision breakdown on DLP-Reactive (\pm std over 5 seeds). [†]HOPE uses a released checkpoint (no seeds). V–V counts contacts between controlled agents; V–Stat counts contacts with static parked cars, curbs, walls, and planters.

C.9 Reward-Mode Control at Inference

Per-agent reward conditioning at training (Appendix A.3) lets the same trained checkpoint be steered along the SR–Coll spectrum at inference time by fixing the goal and collision weights (w_g, w_c) to values within the training sampling range. Table 12 reports three operating points on DLP-Reactive.

The single checkpoint covers an operational range from cautious-and-precise (75.3% SR at 2.0% Coll) to aggressive-and-fast (89.1% SR at 8.7% Coll) without any retraining, providing a deployment-time knob between safety-first and throughput-first regimes. The training-mean default (w_g, w_c) = (1.25, 1.75) reproduces the headline numbers of Table 1 and serves as the balanced operating point between the two extremes. The asymmetric span of the training distribution, with w_c ranging up to 3.0

Reward mode	SR [%]	Coll [%]
Aggressive ($w_c=0.5, w_g=2.0$)	89.1 ± 1.5	8.7 ± 1.0
Mean (default eval)	84.7 ± 1.4	4.1 ± 0.7
Safety ($w_c=3.0, w_g=0.5$)	75.3 ± 1.7	2.0 ± 0.5

Table 12: Reward-conditioning at inference (DLP-Reactive, 5 seeds). The training-mean default reproduces the headline number in Table 1.

while w_g caps at 2.0, is what equips the policy with a wider safety-side margin than throughput-side margin, matching the deployment priority of production-grade parking.